Sensing and Refilling Calcium Stores in an Excitable Cell

Yue-Xian Li,*§ Stanko S. Stojilković,# Joel Keizer,§ and John Rinzel*

*Mathematical Research Branch, National Institute of Arthritis, Diabetes, and Digestive and Kidney Diseases, and #Endocrinology and Reproduction Research Branch, National Institute of Child Health and Human Development, National Institutes of Health, Bethesda, Maryland 20892; and §Institute of Theoretical Dynamics, Section on Neurobiology, Physiology, and Behavior, University of California, Davis, California 95616 USA

ABSTRACT Inositol 1,4,5-trisphosphate (IP_3)-induced Ca^{2+} mobilization leads to depletion of the endoplasmic reticulum (ER) and an increase in Ca^{2+} entry. We show here for the gonadotroph, an excitable endocrine cell, that sensing of ER Ca^{2+} content can occur without the Ca^{2+} release-activated Ca^{2+} current (I_{crac}), but rather through the coupling of IP_3-induced Ca^{2+} oscillations to plasma membrane voltage spikes that gate Ca^{2+} entry. Thus we demonstrate that capacitative Ca^{2+} entry is accomplished through Ca^{2+}-controlled Ca^{2+} entry. We develop a comprehensive model, with parameter values constrained by available experimental data, to simulate the spatiotemporal behavior of agonist-induced Ca^{2+} signals in both the cytosol and ER lumen of gonadotrophs. The model combines two previously developed models, one for ER-mediated Ca^{2+} oscillations and another for plasma membrane potential-driven Ca^{2+} oscillations. Simulations show agreement with existing experimental records of store content, cytosolic Ca^{2+} concentration ($[Ca^{2+}]_i$), and electrical activity, and make a variety of new, experimentally testable predictions. In particular, computations with the model suggest that $[Ca^{2+}]_i$ in the vicinity of the plasma membrane acts as a messenger for ER content via Ca^{2+}-activated K^+ channels and Ca^{2+} pumps in the plasma membrane. We conclude that, in excitable cells that do not express I_{crac}, $[Ca^{2+}]_i$ profiles provide a sensitive mechanism for regulating net calcium flux through the plasma membrane during both store depletion and refilling.

INTRODUCTION

In both excitable and nonexcitable cells, elevations in cytosolic Ca^{2+} concentration ($[Ca^{2+}]_i$) can be achieved via Ca^{2+} release from intracellular Ca^{2+} stores, which are commonly expressed as prominent $[Ca^{2+}]_i$ oscillations. This occurs when neurotransmitters or hormones bind to receptors that promote the production of the Ca^{2+} mobilizing intracellular messenger, inositol 1,4,5-trisphosphate (IP_3) (Berridge, 1993). During such agonist-induced Ca^{2+} mobilization, the content of intracellular Ca^{2+} stores declines, resulting in increased Ca^{2+} entry (Casteels and Droogmans, 1981; Takemura et al., 1989) via a process known as capacitative calcium entry (Putney, 1986). In a number of nonexcitable cells, capacitative entry is believed to occur through a Ca^{2+} release-activated Ca^{2+} channel (CRAC) (Hoth and Penner, 1992; Zweifach and Lewis, 1993). Several hypotheses have been proposed to explain how the store content regulates the CRAC channels, ranging from the existence of diffusible messengers to the interaction between proteins on the endoplasmic reticulum (ER) and the plasma membranes (Berridge, 1995). In excitable cells, however, Ca^{2+} entry through voltage-gated Ca^{2+} channels is essential for refilling internal stores (Stojilković et al., 1992; Jaffe and Brown, 1994), but how store content controls Ca^{2+} entry through these channels has not been clarified. To address this question, we employed the rat pituitary gonadotroph, an excitable endocrine cell, as a model.

Gonadotrophs in culture conditions are capable of firing spontaneous action potentials (APs) (Kukuljan et al., 1992) that generate $[Ca^{2+}]_i$ oscillations with an amplitude of ~100–200 nM (Iida et al., 1991; Rawlings et al., 1991). The ionic basis of this voltage-driven oscillator (plasma membrane oscillator) has been established and analyzed (Stutzin et al., 1989; Tse and Hille, 1993; Li et al., 1995b). Large-amplitude $[Ca^{2+}]_i$ oscillations have also been observed in the presence of the physiological agonist gonadotropin-releasing hormone (GnRH) (Iida et al., 1991; Leong and Thorner, 1991). Such oscillations, caused by episodic Ca^{2+} release from the ER (ER oscillator), were also seen in cells placed in Ca^{2+}-deficient medium (Iida et al., 1991) or clamped at very negative voltages (Kukuljan et al., 1994). Similar oscillations were also induced by injecting IP_3 or its nonmetabolizable derivatives (Tse and Hille, 1992; Stojilković et al., 1993), suggesting that a steady IP_3 signal was sufficient to trigger oscillations. Moreover, ryanodine exerts no influence on the ER oscillator (Stojilković et al., 1994), thus excluding the involvement of ryanodine channels in the ER oscillator in gonadotrophs. Based on these experiments and the biphasic $[Ca^{2+}]_i$ gating of the IP_3 receptor/channels (Iino, 1990; Bezprozvanny et al., 1991; De Young and Keizer, 1992), a mechanistic model was constructed that accounts for the dose dependence of GnRH-induced $[Ca^{2+}]_i$ oscillations (Li et al., 1994).

These and other studies have established gonadotrophs as a prototype for excitable cells that express both voltage- and IP_3-induced $[Ca^{2+}]_i$ oscillators (Stojilković and Catt, 1994). However, several questions concerning the interaction between the ER Ca^{2+} release mechanism and the voltage-

Received for publication 24 June 1996 and in final form 27 November 1996.

Address reprint requests to Dr. John Rinzel, Mathematical Research Branch, NIDDK, National Institutes of Health, 9190 Wisconsin Ave., Suite 350, Bethesda, MD 20814. Tel.: 301-496-4325; Fax: 301-402-0535; E-mail: rinzel@helix.nih.gov.

0006-3495/97/03/1080/12 $2.00

gated Ca^{2+} entry pathway remain unresolved, including the identity of the messenger that communicates the filling state of the stores to the plasma membrane. To explore this and related questions, we combine experimental approaches and computations with a new mathematical model of the two coupled oscillators. We find that our experimental measurements of store content, $[Ca^{2+}]_i$, and plasma membrane voltage can be explained consistently by the interaction between the ER Ca^{2+} release mechanism and plasma membrane electrical activity, with $[Ca^{2+}]_i$ itself playing the role of messenger.

MATERIALS AND METHODS

Computational model

The cell is modeled as a spherical cytosol coexisting with a continuously distributed ER sharing the same cellular volume. The two compartments, the cytosol and ER, are separated by the ER membrane, which contains IP_3 channels, SERCAs (sarco- and endoplasmic reticulum calcium ATPases), and small conductance Ca^{2+} leaks. The cytosol is bounded by a two-dimensional spherical surface, the plasma membrane, at a radius of 10 μm. Located on this surface are a variety of ionic channels and active Ca^{2+} transport proteins, Ca^{2+} ATPases, and Na^+-Ca^{2+} exchangers that pump Ca^{2+} out of the cell against the Ca^{2+} concentration gradient. Ca^{2+} can diffuse in both the cytosol and ER, but with very different diffusion rates (because of different buffering properties). No direct interaction exists between the ER and the extracellular medium. The model is governed by the following set of differential equations and boundary conditions:

$$\frac{\partial C}{\partial t} = j_{rel} - j_{fil} + D\nabla^2 C \qquad \text{in cytosol} \quad (1)$$

$$\frac{\partial C_{er}}{\partial t} = -\sigma^{-1}(j_{rel} - j_{fil}) + D_{er}\nabla^2 C_{er} \qquad \text{in ER} \quad (2)$$

$$D_o \frac{\partial C}{\partial r}\bigg|_{r=R} = j_{in} - j_{out} = -\alpha[I_{Ca-T} + I_{Ca-L}] - j_{out} \qquad (3)$$

at cell surface

$$\frac{\partial C_{er}}{\partial r}\bigg|_{r=R} = 0 \quad (4)$$

where C and C_{er} represent $[Ca^{2+}]_i$ and $[Ca^{2+}]_{ER}$, respectively; j_{rel} and j_{fil} (in $\mu M \cdot s^{-1}$) are the flux densities of ER Ca^{2+} release and uptake (taking into account the buffering capacity of the cytosol); j_{in} and j_{out} (in $\mu M \cdot \mu m \cdot s^{-1}$) are the flux densities of Ca^{2+} entry and extrusion across the plasma membrane, and $j_{pm} = j_{in} - j_{out}$ is the net flux. D and D_{er} are the respective Ca^{2+} diffusion coefficients in the cytosol and the ER, and D_0 is the Ca^{2+} diffusion coefficient in buffer-free medium. The ratio between the effective volumes of the ER and the cytosol is $\sigma = (V_{er}/f_{er})/(V_{cyt}/f_{cyt})$, where f_{er} and f_{cyt} are, respectively, the Ca^{2+} buffering coefficients (free over total $[Ca^{2+}]$) in the ER and cytosol. The parameter $\alpha = 1/(2FA_{cell}) = 4.144\ \mu M \cdot \mu m/(s \cdot pA)$, where F is Faraday's constant and A_{cell} is the cell's surface area, converts inward Ca^{2+} current into Ca^{2+} influx density. Parameter values and definitions of the functions are given in the Appendix.

For simplicity, we assume spherical symmetry in the distribution of ion channels and pumps on the plasma membrane and in the distribution of the ER, the IP_3R channels, the leaks, and the SERCA pumps in the cytoplasmic volume. Therefore, Ca^{2+} diffuses only in the radial direction. Thus the Laplacian ∇^2 is simplified to $r^{-2}\partial_r(r^2\partial_r)$.

Constraints on the parameter values

Pituitary gonadotrophs are well characterized quantitatively in terms of both their electrophysiology and agonist-induced calcium signaling (see review by Stojilković and Catt, 1994). In a series of papers (Li et al., 1994, 1995b) we have developed the model using available experimental data that tightly constrain many of the parameter values. Several parameters have been measured directly in gonadotrophs, including cell size, Ca^{2+} buffering capacity, ER store content, Ca^{2+}-mediated inactivation kinetics of IP_3 channels, and those associated with the plasma membrane electrical oscillator (see Li et al., 1995b, for detailed reference to the experimental source of these parameters). Some parameter values have been adapted from experiments on other cell types. These include parameters such as the Ca^{2+} diffusion coefficient in the cytosol and those associated with the Ca^{2+} sensitivity of SERCA and plasma membrane Ca^{2+} pumps, and of the IP_3R. A few remaining parameter values are indirectly constrained by other known parameters so as to systematically reproduce the observed dynamic patterns. For example, the ER's Ca^{2+} diffusion coefficient is unknown; we assume it to be 25% of that in the cytosol. However, the results change little when the value zero is used instead. In the absence of information to the contrary, we have made the idealizing assumption that the ER store is distributed homogeneously throughout the cell volume. Although large intracellular compartments like the nucleus are known not to contain ER, Ca^{2+} appears to travel without much restriction through the nucleus (Lin et al., 1994). Thus this assumption probably does not introduce significant errors.

Numerical method

Replacing variables C and C_{er} by $U = rC$ and $W = rC_{er}$ in Eqs. 1–4, we transform the diffusion terms into $\partial^2 U/\partial r^2$ and $\partial^2 W/\partial r^2$. The problem reduces to a reaction-diffusion equation in one space dimension, with time-dependent boundary conditions governed by the voltage equation. The space is discretized into 50 equal-spaced segments, i.e., 50 concentric shells of equal thickness $\delta r = 0.2$ μm. The second derivative $\partial^2 Y/\partial r^2$ is then discretized as $(Y_{j+1} - 2Y_j + Y_j - 1)/\delta r^2$, where Y represents U and W; j denotes the numbering of shells. The discretized ordinary differential equations are then solved with the fourth-order Runge-Kutta method by using a fixed time step $\delta t = 0.5$ ms.

Experimental procedures

Gonadotrophs were prepared by enzymatic dispersion of anterior pituitary glands obtained from ovariectomized rats (Stojilković et al., 1990). Cells were incubated in medium 199 at 37°C in 5% CO_2/95% air and were used in measurements 48–72 h after plating. Plasma membrane voltage and $I_{K(Ca)}$ were measured by the nystatin-perforated patch-clamp technique, as described by Kukuljan et al. (1994). In Ca^{2+} measurements, enriched pituitary gonadotrophs were plated in 35-mm Petri dishes containing 25-mm round glass coverslips coated with 0.01% poly-L-lysine. Cells were loaded with 1 μM Indo 1-AM (Molecular Probes, Eugene, OR) for 60 min at 37°C, and mounted on the stage of an inverted Diaphor microscope attached to a Nikon intracellular Ca^{2+} analysis system. $[Ca^{2+}]_i$ values were calculated with a standard calibration curve that was constructed by adding various doses of Ca^{2+} to 10 μM Indo-1. The kinetics of pool depletion were evaluated in cells placed in Ca^{2+}-deficient medium. The cells were first stimulated with 100 nM GnRH followed by the application of 1 μM ionomycin at different times (50–400 s) after the onset of the GnRH signal. Pool refilling was evaluated in cells first challenged by 100 nM GnRH for 10 min in Ca^{2+}-deficient medium to deplete the ER Ca^{2+} content. Then the stimulus was removed by washing, and normal Ca^{2+} concentration (2.5 mM) was recovered in the medium to initiate store refilling. Ionomycin (1 μM) was applied at different times after refilling began. The amplitude of the ionomycin-induced Ca^{2+} release, expressed as a percentage of the response amplitude to the same dose of ionomycin in cells not subjected to previous GnRH stimulation, was used as an estimate of the relative store content.

RESULTS

Fig. 1 *A* shows a typical firing pattern recorded in gonadotrophs before and during the stimulation by a physiological dose of GnRH. The regularly spaced APs, observed before GnRH was applied, were replaced by a burst firing pattern after the addition of GnRH (*open arrow*). Simultaneous records of voltage and $[Ca^{2+}]_i$ showed that the interburst hyperpolarization was caused by pulses of Ca^{2+} released from internal stores that activate a Ca^{2+}-dependent K^+ current $I_{K(Ca)}$ (Kukuljan et al., 1992; Tse and Hille, 1992). This was reaffirmed by switching from current- to voltage-clamp (*filled arrow*), which eliminated the voltage spikes but retained oscillatory changes in the current.

Fig. 1 *B* shows the computed time course of voltage (*top panel*), $I_{K(Ca)}$ (*middle panel*), and $\overline{[Ca^{2+}]_i}$ (*lower panel*); where $\overline{[Ca^{2+}]_i}$ denotes the spatially averaged $[Ca^{2+}]_i$ over the entire cell. In addition to reproducing the experimental records, the computations expose the difference between the $I_{K(Ca)}$ profiles under current- and voltage-clamp conditions. A direct comparison with experiment is not yet possible, because there is no way to measure $I_{K(Ca)}$ under current-clamp condition. In the middle panel of Fig. 1 *B* the increase in $I_{K(Ca)}$ during $[Ca^{2+}]_i$ spikes under current clamp is small when compared to the one that occurs when the cell is voltage-clamped at −50 mV due to the difference in the K^+ driving force. When the cell is clamped at a voltage near the K^+ reversal potential, $I_{K(Ca)}$ is also small (not shown). Because all of the ionic currents are small in the polarized phases (Li et al., 1995b), it does not take a large $I_{K(Ca)}$ to keep the cell polarized. Therefore, voltage clamp simplifies the response by eliminating the dynamic interactions between plasma membrane electrical activity and ER-mediated $[Ca^{2+}]_i$ oscillations. Such interactions are crucial in coordinating voltage-gated Ca^{2+} entry and Ca^{2+} release from the ER.

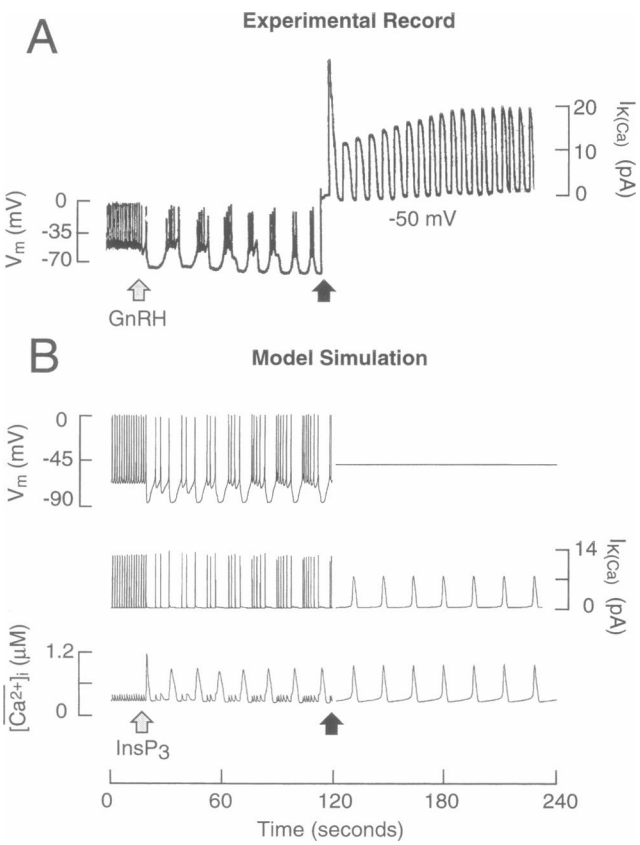

FIGURE 1 GnRH-induced responses in current and voltage-clamp conditions, experimental record (*A*) and model simulation (*B*). Transition from tonic spiking to bursting was induced, at the open arrow, by the application of 1 nM GnRH (*A*) and 0.3 μM IP_3 (*B*). Starting at the filled arrow, voltage clamp at −50 mV was applied. Also plotted in *B* are the temporal profiles of $I_{K(Ca)}$ (*middle*) and $\overline{[Ca^{2+}]_i}$ (*bottom*). $\overline{[Ca^{2+}]_i}$ denotes the average of $[Ca^{2+}]_i$ over the whole cellular space.

The ability of the model to reproduce, in a systematic way, the observed voltage responses to a wide range of GnRH doses without readjusting other parameters is illustrated in Fig. 2. In the left column of Fig. 2, the experimental dose response to GnRH is shown. Model simulations given in the right column reproduce the observed voltage dose response, using IP_3 as a parameter that is experimentally related to [GnRH] by a log-linear relationship (Stojilković, unpublished observations). Probably because of the small size of gonadotrophs, the same agonist dose often triggers somewhat different responses in different cells (cf. the first four experimental records in Fig. 2). However, the dose-response scenario plotted in Fig. 2 is representative of hundreds of similar observations (Li et al., 1994). As shown in Fig. 1 *B*, the number of spikes per burst is determined by the interval between $[Ca^{2+}]_i$ pulses; when $[Ca^{2+}]_i$ oscillates at a high frequency, the voltage is forced to oscillate at a polarized level with small amplitude (see Fig. 2, *second panel from bottom*). Hyperpolarization immediately after the onset of high-dose stimuli (*the two bottom panels*) is associated with the first phase of a biphasic $[Ca^{2+}]_i$ response. The duration of this first phase decreases as the agonist dose increases, consistent with earlier results of $[Ca^{2+}]_i$ dose response in gonadotrophs (Li et al., 1994). In both the observed and simulated responses, two general features emerge: the frequency of voltage spikes is 1) greatly reduced upon the addition of stimulus but 2) gradually increases as time proceeds.

Store depletion and refilling in the absence of I_{CRAC}

To assess the impact of GnRH-induced electrical activity on store content, we carried out simulations like that in Fig. 3 in which the time courses of V, $\overline{[Ca^{2+}]_i}$, and the average of $[Ca^{2+}]_{ER}$ over the entire cell, $\overline{[Ca^{2+}]_{ER}}$, are shown before, during, and after $[IP_3]$ was raised from 0.01 (basal) to 0.42 μM for 5 min. The dotted vertical lines divide the dynamic behavior into four distinct phases: SS-1 (Steady-State-1), T-1 (Transient-1), SS-2 (Steady-State-2), and T-2 (Transient-2).

SS-1 is the long-term behavior of the model cell in the absence of agonist. During each voltage cycle, the net Ca^{2+}

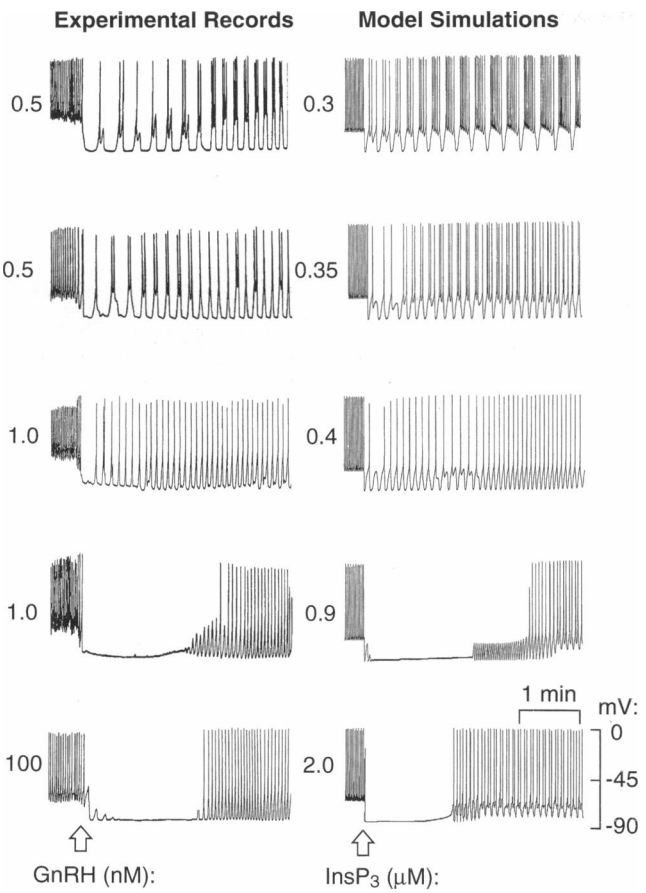

FIGURE 2 Dose-dependent voltage response profiles, experimental records (*left column*), and model simulations (*right column*). In experiments, increasing doses of GnRH were applied at the arrow. In model simulations, increasing doses of IP_3 were used, implicitly assuming that a higher GnRH dose results in a higher IP_3 production rate. At the arrow, IP_3 was switched instantaneously from a basal level (0.01 μM) to the levels marked by the number to the left of each curve. The $[IP_3]$ values in the right column give the actual parameter values used in the simulations and by no means represent the realistic functional relationship between the GnRH dose and the corresponding level of IP_3.

exchange is zero across both the ER and the plasma membranes. In one cycle 0.03 fmol of Ca^{2+} enters the cell, while the same amount of Ca^{2+} is extruded by plasma membrane Ca^{2+} pumps. Furthermore, per cycle, 0.57 fmol of Ca^{2+} leaves the ER and the same amount enters the ER via the SERCA pumps. Tonic spiking in SS-1 sustains the $\overline{[Ca^{2+}]_i}$ oscillations with a frequency of 0.8 Hz and an amplitude of 120 nM. SS-1 is the full-store state in which Ca^{2+}_{ER} fluctuates only slightly around its high (67 μM) level, implying a total Ca^{2+} concentration (free plus buffered) in the ER of 27 mM, as measured by the ER volume.

The phase T-1 starts (and SS-1 ends) when $[IP_3]$ is increased. Fig. 3 shows that the ER store depletes during T-1, owing to both increased Ca^{2+} extrusion and decreased Ca^{2+} entry. For example, during the fourth cycle after $[IP_3]$ addition, 4 fmol of Ca^{2+} is released from the ER and 3.4 fmol enters, causing $\overline{[Ca^{2+}]_{ER}}$ to drop by 2.4 μM. (3.6% of basal). Of the 0.6 fmol net Ca^{2+} lost by the ER, 40% of this amount leaves the cell and 60% contributes to raising cycle-averaged $\overline{[Ca^{2+}]_i}$. Notice that during T-1, the minimum value of $[Ca^{2+}]_i$ during an oscillation progressively declines below the basal level as the store content declines. This results in a decrease in baseline $I_{K(Ca)}$ that causes a slight depolarization and an increase in voltage spiking rate.

After about 4 min, SS-2 is reached, ending T-1, when the net Ca^{2+} exchange per cycle across the ER and the plasma membranes again vanishes, owing to the gradual recovery of Ca^{2+} entry and reduced Ca^{2+} extrusion as the store content declines. Thus SS-2 is the empty-store state with less than 10% of the store content at SS-1, for $[IP_3]$ greater than 0.4 μM (see Fig. 4 *A*). This state persists as long as $[IP_3]$ remains elevated and extracellular Ca^{2+} concentration is unchanged. Full-store content cannot be restored in SS-2, despite an AP rate comparable to that in SS-1, because IP_3R Ca^{2+} permeability is increased by higher $[IP_3]$. Although $\overline{[Ca^{2+}]_i}$ varies around a level similar to basal (*horizontal dashed line in middle panel* of Fig. 3), the spatiotemporal profile of $[Ca^{2+}]_i$ and the firing pattern of APs differ in the two states (see Fig. 5).

The store-refilling phase, T-2, starts when $[IP_3]$ is reduced to basal level. In Fig. 3 this creates a transient decline in $[Ca^{2+}]_i$. With this decline, the plasma membrane fires APs faster (4–5 Hz), thus accelerating Ca^{2+} entry. During T-2 the per-spike Ca^{2+} entry is almost fixed (~0.03 fmol), but per-spike Ca^{2+} extrusion is reduced because of decreased $[Ca^{2+}]_i$, resulting in net Ca^{2+} entry per voltage cycle. Thus, during the fourth AP cycle after the removal of IP_3, the cell gains a net 0.023 fmol Ca^{2+}, much of which is taken up by the ER. In simulations, pool-refilling occurs when $[Ca^{2+}]_i$ is below basal level. By the end of T-2, the basal level of SS-1 is recovered, full store content is restored, and a reduced firing rate balances the Ca^{2+} exchanges across the ER and the plasma membranes. In this simulation, T-2 was initiated by an instantaneous reduction of $[IP_3]$ although the measured decline in $[IP_3]$ after GnRH withdrawal follows an exponential time course with a half-time of ~1 min or longer (Morgan et al., 1987). When simulations employed an exponential decrease in $[IP_3]$ (not shown), the resulting decline in $[Ca^{2+}]_i$ was less obvious. During the gradual decrease in $[IP_3]$, $[Ca^{2+}]_i$ first slowly declines and starts to increase later. As a consequence, the membrane firing rate first slowly increases and then progressively decreases. In Fig. 3, instantaneous withdrawal of $[IP_3]$ was used to clearly demonstrate the $[Ca^{2+}]_i$ decline after the withdrawal of the stimulus.

The simulations suggest that the closure of IP_3 channels is the trigger for pool refilling. As discussed below, the increase in $[Ca^{2+}]_i$ after $[IP_3]$ increase in the simulations, as well as the decrease in $[Ca^{2+}]_i$ after IP_3 withdrawal, is sufficient to report the ER content to the plasma membrane. Thus in gonadotrophs a reduction in $[Ca^{2+}]_i$ appears sufficient to promote net Ca^{2+} entry, whereas high $[Ca^{2+}]_i$ seems not only unnecessary but also potentially detrimental

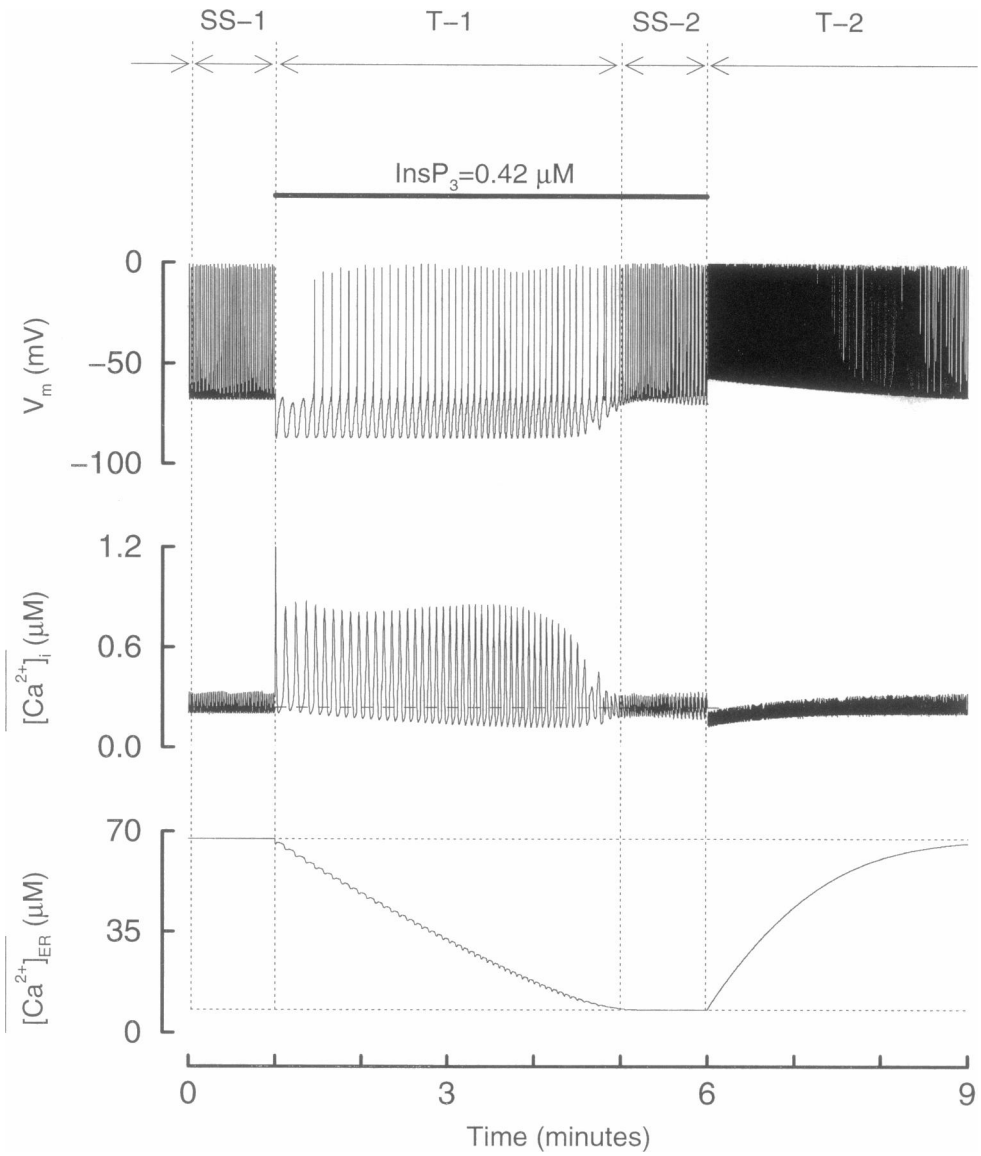

FIGURE 3 The store-depleting phase (T-1) and the store-refilling phase (T-2) are two transients linking the full-store state (SS-1) and the empty-store state (SS-2). These four phases are divided by the four vertical dashed lines. T-1 and T-2 are abbreviations for Transient-1 and Transient-2, repectively, and SS-1 and SS-2 stand for Steady State-1 and Steady State-2. The transition from SS-1 to T-1 was initiated by an instantaneous switch of $[IP_3]$ from 0.01 μM (basal) to 0.42 μM. The transition from SS-2 to T-2 was caused by switching $[IP_3]$ from 0.42 μM back to the basal level. The simulation was started at basal IP_3 level and when the model cell was already in SS-1.

to pool refilling. Although simultaneous recording of $[Ca^{2+}]_i$, $[Ca^{2+}]_{ER}$, and V is not yet experimentally feasible, different aspects of Fig. 3 have been observed in separate measurements. Thus simultaneous recordings of V and $\overline{[Ca^{2+}]_i}$ have been obtained during the SS-1 phase and show agreement with model simulations (Li et al., 1995b). The voltage variations during the first few minutes of T-1 have long been observed (Kukuljan et al., 1992; Stojilković et al., 1992; see also Fig. 2), as well as $\overline{[Ca^{2+}]_i}$ oscillations during the same period of time (see, e.g., Iida et al., 1991). The gradual decline of the minimum value of $[Ca^{2+}]_i$ during T-1 and the transient drop in $[Ca^{2+}]_i$ after IP_3 withdrawal has not been detected fluorometrically. Nevertheless, records of $I_{K(Ca)}$ under voltage-clamp conditions appear to indirectly support the decline of $[Ca^{2+}]_i$ below its basal level as the store content declines and after GnRH is withdrawn (Tse et al., 1994b). Simulations under voltage-clamp conditions of this model reproduce those experiments with good agreement (not shown). The durations of both T-1 and T-2 in Fig. 3, although computed under current-clamp conditions, match well with the experimental observations. Thus the simulation in Fig. 3 shows good agreement with the limited data currently available and reveals for the first time four distinct dynamic phases of Ca^{2+} signaling in gonadotrophs and the transitions between them.

Dose dependence of store depletion and refilling

To further explore the mechanism of store refilling, we have examined its dependence on the stimulus dose. The time dependence of store depletion computed for five values of $[IP_3]$ is plotted in Fig. 4 *A*. The half-depletion time (*vertical dashed lines*) decreases as the stimulus dose increases. In addition, the percentage decrease in $\overline{[Ca^{2+}]_{ER}}$ at the end of depletion is greater for higher doses, saturating at ~95% for

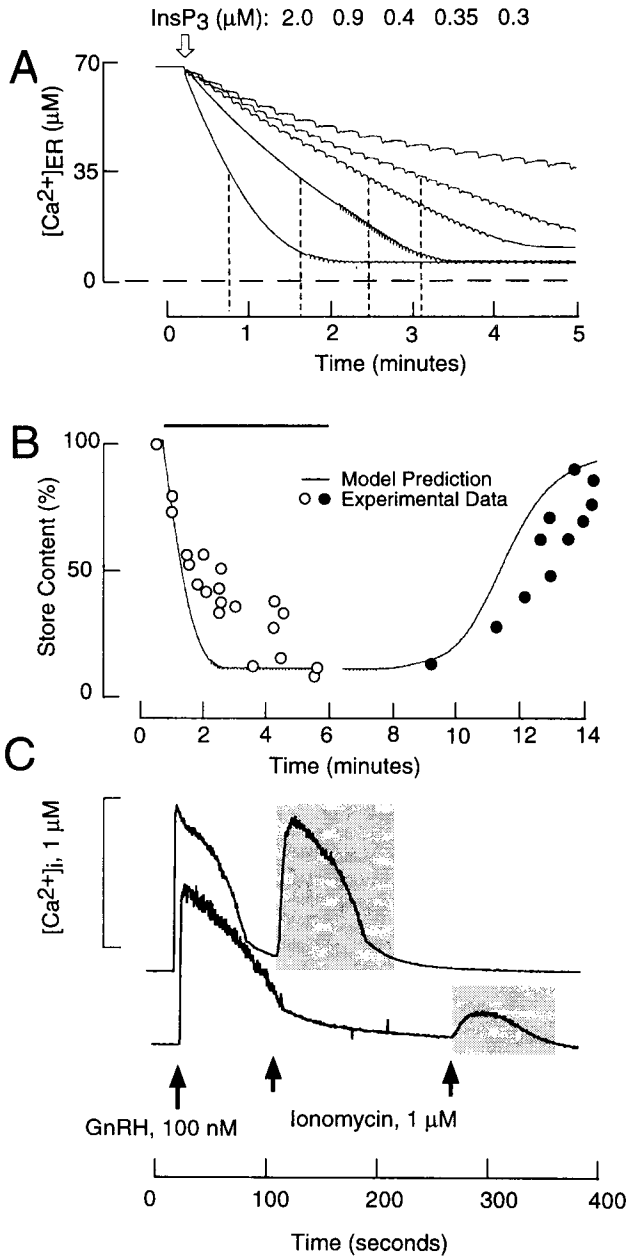

FIGURE 4 Dose dependence of store depletion and refilling. (*A*) Model simulated $[Ca^{2+}]_{ER}$ transient profiles during depletion phase, T-1, for increasing IP_3 doses (*from top to bottom*). (*B*) Comparison between recorded store depletion (○) and refilling (●) profiles and the corresponding profiles obtained in model computation. In *A*, a step increase in IP_3 from the basal to the marked values occurs at the moment indicated by the arrow. The vertical dotted lines indicate the time when the store reaches half its prestimulus level. In *B*, the store content is expressed as a percentage of the prestimulus $[Ca^{2+}]_{ER}$. The store depletion is simulated with $[IP_3] = 2$ μM and $[Ca^{2+}]_o = 5$ μM. The store refilling is computed by withdrawing the IP_3 signal exponentially with a 2-min decay time and with $[Ca^{2+}]_o = 2.5$ mM. See Experimental Procedures for details of the experimental methods. (*C*) Two examples of experiments in which store content was measured. In cells bathed in Ca^{2+}-deficient medium, ionomycin was applied at different times after GnRH stimulation. Data were normalized using GnRH (100 nM)-induced Ca_i^{2+} response as 100%.

IP_3 doses higher than 0.8 μM. This phenomenon has been refered to by some researchers as "quantal" Ca^{2+} release (Bootman, 1994). The IP_3 dose also changes the dynamic features of $[Ca^{2+}]_{ER}$ during the oscillatory T-1 phases. At low $[IP_3]$ the $[Ca^{2+}]_{ER}$ cycle (Fig. 4 *A*, *upper curve*) is characterized by a sharp drop and a slow recovery, whereas at higher $[IP_3]$ the cycle involves both a sharp drop and a sharp recovery. These differences are largely due to the differences in the frequency of $[Ca^{2+}]_i$ oscillations and the instantaneous store content.

Fig. 4 *B* compares the simulated time dependence of store depletion and refilling with that obtained using ionomycin and the method illustrated in Fig. 4 *C*. The calculated refilling curves for other stimulus doses are qualitatively similar to that shown in Fig. 4 *B*, except that the refilling starts from different levels of depletion. The semiquantitative agreement between simulation and measurement reinforces our confidence in the simulations.

Coordination between Ca^{2+} release and voltage spikes

As demonstrated in a previous study (Li et al., 1995b), the lumped-cytoplasm approximation, which assumes that immediately after entering the cell Ca^{2+} ions instantaneously spread throughout the entire cytoplasm, fails to explain the frequency of spontaneous AP spiking in gonadotrophs. In particular, the characteristic after-hyperpolarization at the end of a spike has been explained (Li et al., 1995b) by the localized increase in $[Ca^{2+}]_i$ at the plasma membrane before its diffusion into the bulk cytoplasm. Here we further explored the spatiotemporal variation of $[Ca^{2+}]_i$ and its coordination with membrane potential (Fig. 5). Three sets of panels are used to characterize store release during SS-1 (Fig. 5 *A*), T-1 (Fig. 5 *B*), and SS-2 (Fig. 5 *C*): in each set, the left panel is for $[Ca^{2+}]_i$, the middle for voltage, and the right for $[Ca^{2+}]_{ER}$. Calculations were carried out for a spherical cell of radius $r = 10$ μm with plasma membrane currents uniformly distributed at the surface. Note that the plasma membrane side of both the $[Ca^{2+}]_i$ and the $[Ca^{2+}]_{ER}$ panels is oriented toward the center. Gray-scale calibration bars are given at the bottom. In SS-1 the voltage-driven Ca^{2+} increases are localized near the plasma membrane. Each AP (seen as a *dark line* in the *middle panel*) produces a sharp $[Ca^{2+}]_i$ spike near the cell surface, where the amplitude of $[Ca^{2+}]_i$ can reach 0.6 μM. These $[Ca^{2+}]_i$ pulses spread to the cell center in about 0.3 *s* with remarkable attenuation in amplitude. The Ca^{2+} exchange across the ER membrane is small and occurs mostly near the plasma membrane.

During the T-1 phase, voltage spikes coordinate with massive ER Ca^{2+} release that occurs throughout the cellular space (Fig. 5 *B*). $[Ca^{2+}]_i$ at the plasma membrane acts on the K(Ca) channels, hyperpolarizing the cell and inhibiting voltage spikes. Only after a delay of several seconds is the membrane again electrically active. Ca^{2+} entry during one

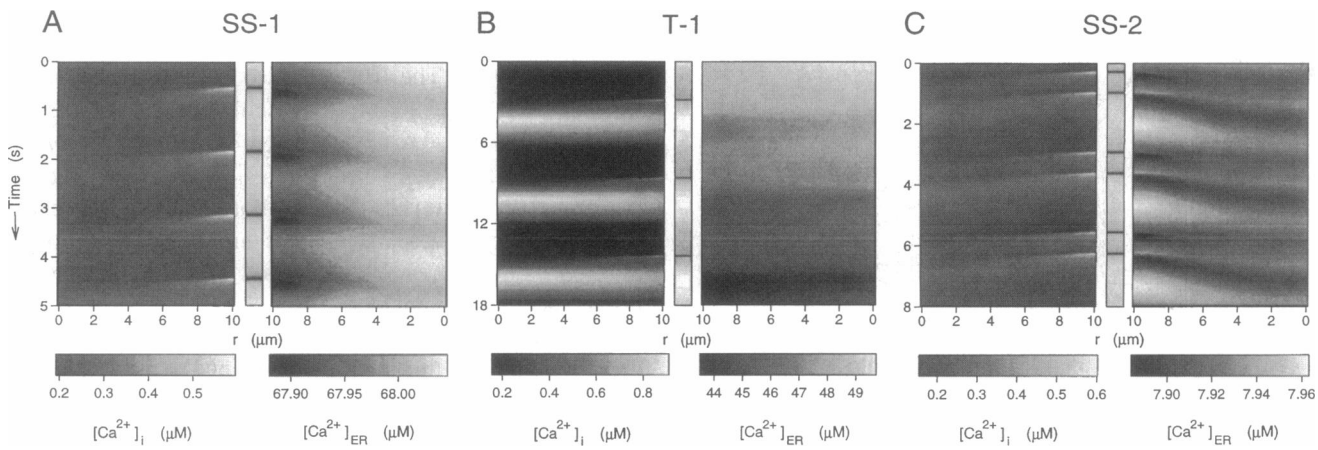

FIGURE 5 Spatiotemporal profiles during the full-store state, SS-1 (*A*); during the store-depleting phase, T-1 (*B*); and during the empty-store state, SS-2 (*C*). Three panels are used for characterizing each of the three phases: the left panel for $[Ca^{2+}]_i$, the middle for voltage, and the right for $[Ca^{2+}]_{ER}$. Scales for $[Ca^{2+}]_i$ and $[Ca^{2+}]_{ER}$ are given by the scale bar below each panel. The voltage varies between 0 (black) and −90 mV (white). Time proceeds vertically, following the downward arrow. The horizontal coordinate, r, denotes the radial distance from the cell center ($r = 0$) to the cell surface ($r = 10$ μm). The plasma membrane side of the panels for both $[Ca^{2+}]_i$ and $[Ca^{2+}]_{ER}$ is directed toward the voltage panel in the middle. Parameter values are same as in Fig. 3. *B* and *C* were obtained at 1 and 10 min, respectively, after T-1 was initiated.

voltage spike triggers the next pulse of Ca^{2+} release from the store. In this case, there is a one-to-one correspondence between voltage spikes and Ca^{2+} release pulses, which gives rise to the stepwise depletion of the store (Fig. 5 *B*, *right panel*) with only partial recovery between successive $[Ca^{2+}]_i$ pulses. When SS-2 is reached (Fig. 5 *C*), APs reorganize into bursts of two spikes. The reason that two APs can now occur within a fraction of a second is that because of store depletion, Ca^{2+} entry during a single AP can no longer release sufficient Ca^{2+} to prevent the cell from rapidly firing another AP. However, the net $[Ca^{2+}]_i$ increase at the plasma membrane caused by two closely spaced APs is able to hyperpolarize the cell for a longer period of time. As in SS-1, increases in $[Ca^{2+}]_i$ are localized near the cell surface, whereas $[Ca^{2+}]_{ER}$ is nearly uniform.

Electrical activity is essential in sustaining pulsatile ER Ca^{2+} release in the empty-store state (SS-2). When $[IP_3] = 0.3$ μM, six pairs of AP spikes occur during the long

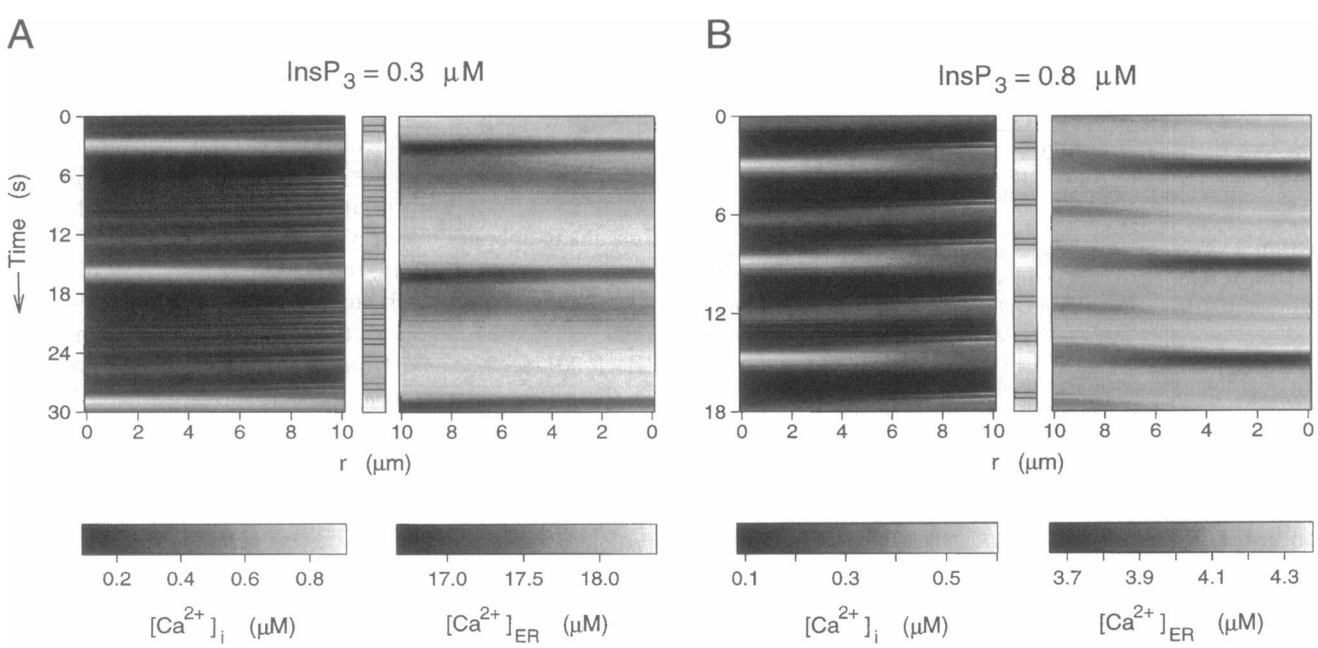

FIGURE 6 Spatiotemporal profiles showing the role of voltage spikes in sustaining ER Ca^{2+} excitability in the empty-store state (SS-2) for $IP_3 = 0.3$ μM (*A*) and $IP_3 = 0.8$ μM (*B*). The three panels in each set are arranged as in Fig. 5. The scales are also defined in the same way. Notice that in *A*, the peak ER Ca^{2+} release in the cell center clearly precedes the peak release near the cell surface.

intervals between $[Ca^{2+}]_i$ pulses (Fig. 6 *A*). The accompanying Ca^{2+} entry substantially reduces the speed and the extent of store depletion (cf. Fig. 4 *A*), which ceases when the ER content is near 17 μM. At this content, the ER retains its ability to generate large-amplitude $[Ca^{2+}]_i$ pulses, suggesting that the plasma membrane electrical activity is able to sustain oscillatory Ca^{2+} release from the ER when the oscillation frequency is low. Simulations demonstrate that a dozen AP spikes just suffice to compensate the loss of 0.22 fmol Ca^{2+} by the ER during each oscillation period.

On the other hand, Fig. 6 *B* shows a case in which a 94% (from 67 to 4 μM) ER depletion occurs when SS-2 is reached. After such drastic depletion, the ER still retains its ability to generate pulses of Ca^{2+} release with an amplitude near 600 nM. Here voltage firing is again characterized by periodic bursts of pairs of APs. The first pair of APs reloads the ER to a level needed for generating the ER discharge, and the second discharges it. In some other cases, voltage spikes can only generate brief $[Ca^{2+}]_i$ pulses near the cell surface (Fig. 5, *A* and *C*). Again, this result shows that during sustained stimulation at high agonist doses, voltage-driven Ca^{2+} entry is essential in maintaining the ER oscillator by partially reloading the store and by triggering release.

Communication between the ER and plasma membrane via cytosolic calcium

Fig. 7 *A* illustrates that the ER content during depletion and refilling is tightly coupled to Ca^{2+} flux across the cell surface. There $[\overline{Ca^{2+}}]_{ER}$ is calculated as a function of time during depletion and refilling (cf. Fig. 3) by averaging $[Ca^{2+}]_{ER}$ over the cell and over each voltage spike. The net Ca^{2+} flux across the plasma membrane, $\overline{j_{pm}}$, averaged over the same voltage spike is plotted versus $[\overline{Ca^{2+}}]_{ER}$. In SS-1 and SS-2 (*filled and open circles*, respectively), the average flux is zero. Application of IP_3 (+ *arrow*) initiates store depletion (T-1), which is also characterized by net Ca^{2+} extrusion ($\overline{j_{pm}}$ negative). Note that after a brief transient after the addition of IP_3, the net Ca^{2+} efflux decreases monotonically ($\overline{j_{pm}}$ less negative) as store content declines. This decrease is due primarily to the decline of the mean plasma membrane efflux that dominates the smaller and nearly constant mean voltage-gated influx (0.01 fmol/s). The abrupt withdrawal of IP_3 (− *arrow*) initiates store refilling (T-2) and Ca^{2+} entry ($\overline{j_{pm}}$ positive). Again, the net Ca^{2+} influx rate is a monotonic function of ER content: the lower the content, the higher the net influx rate. During T-2 the mean influx rate dominates mean efflux, which is nearly constant (0.03 fmol/s).

In addition to revealing that store content correlates with Ca^{2+} flux across the plasma membrane, model computations suggest that Ca^{2+} carries the message through its spatiotemporal profile. The way we study this problem is to compare the changes in Ca^{2+} entry as a function of store content (Fig. 7 *A*) to the corresponding changes of a variety

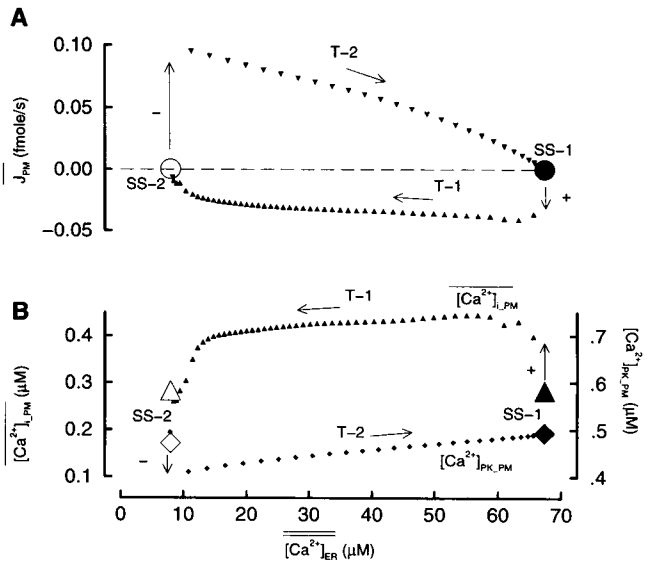

FIGURE 7 The ER store content, $[\overline{\overline{Ca^{2+}}}]_{ER}$, controls the net Ca^{2+} flux across the plasma membrane, J_{PM} (*A*), by controlling the average ($[\overline{Ca^{2+}}]_{i\_PM}$) and the peak value ($[Ca^{2+}]_{PK\_PM}$) of $[Ca^{2+}]_i$ near the plasma membrane (*B*). Dynamic transition between the successive phases, SS-1, T-1, SS-2, and T-2, are plotted following the direction of the arrows. $[\overline{\overline{Ca^{2+}}}]_{ER}$ is obtained by averaging $[Ca^{2+}]_{ER}$ over the cellular space and over each voltage oscillation cycle during each of the four phases. $[\overline{Ca^{2+}}]_{i\_PM}$ is calculated as the $[Ca^{2+}]_i$ near the plasma membrane averaged over each voltage cycle. The large filled circle (or triangle or diamond) represents the SS-1 or full-store state, and the corresponding open symbol denotes the SS-2 or empty-store state. The vertical arrows marked by a plus sign indicate the instantaneous addition of IP_3, and those marked by a minus sign denote the instantaneous withdrawal of IP_3. The IP_3 value jumps between 0.42 and 0.01 μM at these arrows. The horizontal arrows indicate the direction of time evolution in the respective phase. In *B*, the triangles denote $[\overline{Ca^{2+}}]_{i\_PM}$, and the diamonds denote $[Ca^{2+}]_{PK\_PM}$.

of spatiotemporal Ca^{2+} signals, including average and peak values of $[\overline{Ca^{2+}}]_i$ at the plasma membrane over each voltage spike ($[\overline{Ca^{2+}}]_{i\_PM}$ and $[Ca^{2+}]_{PK\_PM}$; see Fig. 7 *B*) as well as $[Ca^{2+}]_i$ averaged over the entire cytosolic space and over each voltage spike ($[\overline{\overline{Ca^{2+}}}]_i$). Simulations also indicate that variations in average and peak values of $I_{K(Ca)}$ over each voltage spike are qualitatively identical to those of $[\overline{Ca^{2+}}]_{i\_PM}$ and $[Ca^{2+}]_{PK\_PM}$, respectively (not shown). We first compared changes in $[\overline{Ca^{2+}}]_{i\_PM}$ and $[Ca^{2+}]_{PK\_PM}$, which are directly linked to the plasma membrane, to changes in Ca^{2+} entry. After a brief transient at the beginning of the T-1 phase, the monotonic decrease in $[\overline{Ca^{2+}}]_{i\_PM}$ (Fig. 7 *B*, *upward triangles*) mirrors the monotonic increase in net Ca^{2+} influx (Fig. 7 *A*, *upward triangles*). This contrasts with $[Ca^{2+}]_{PK\_PM}$, which has an N-shaped rather than monotonic behavior during T-1 (not shown). During T-2, however, the monotonic increase in $[Ca^{2+}]_{PK\_PM}$ (Fig. 7 *B*, *diamonds*) coincides with the monotonic decrease in Ca^{2+} influx (Fig. 7 *A*, *downward triangles*), whereas $[\overline{Ca^{2+}}]_{i\_PM}$ increases and then decreases before the T-2 phase ends (not shown). Finally, $[\overline{\overline{Ca^{2+}}}]_i$, which is a measurable variable that does not influence the plasma

membrane directly, correlates very well during T-1 with $[Ca^{2+}]_{i\_PM}$, but during T-2 it first increases and then decreases as the store content approaches its full-store level. These results point to $[Ca^{2+}]_{PK\_PM}$ (or peak value of $I_{K(Ca)}$) as the signal responsible for the monotonic decrease in Ca^{2+} entry as the store refills.

These studies suggest that during T-1 the regulation of net Ca^{2+} efflux is primarily due to $[Ca^{2+}]_{i\_PM}$, which controls Ca^{2+} extrusion by plasma membrane Ca^{2+} pumps. Owing to the occurrence of large-amplitude $[Ca^{2+}]_i$ pulses in T-1, the pumps generate higher Ca^{2+} efflux that prevails over the nearly constant voltage-gated Ca^{2+} influx. During T-2, on the other hand, the peak value of $[Ca^{2+}]_i$ near the plasma membrane controls the rate of AP firing through its influence on $I_{K(Ca)}$, causing influx to decline as the stores refill. In contrast, the value of $[Ca^{2+}]_{i\_PM}$ (or $I_{K(Ca)}$) averaged over a spike does not increase monotonically during T-2. Because $[Ca^{2+}]_{i\_PM}$ is lower than its basal level in T-2, the efflux rate is also below the basal level. However, the rate of AP firing is much higher, causing more Ca^{2+} entry than the suppressed plasma membrane efflux mechanisms can handle, thus allowing more Ca^{2+} to enter the ER. Because the rate of AP-driven Ca^{2+} entry is roughly proportional to the firing rate, Ca^{2+} control of Ca^{2+} influx is mostly accomplished through control of the rate of AP firing. This can be clearly seen in Fig. 3. Communication of the filling state of the store to the plasma membrane, therefore, involves two distinct features of $[Ca^{2+}]_i$ localized near the cell surface: during depletion the decline in average Ca^{2+} decreases Ca^{2+} extrusion via pumps and exchangers, whereas during refilling the slow increase in peak Ca^{2+} slowly reduces voltage-gated Ca^{2+} entry.

DISCUSSION

Agonist-induced Ca^{2+} signaling in electrically excitable cells involves complex interactions among the ER, the cytosol, the plasma membrane, and probably other compartments. Recent experiments with gonadotrophs have provided detailed knowledge regarding $[Ca^{2+}]_i$ changes (Shangold et al., 1988; Iida et al., 1991), plasma membrane voltage V (Kukuljian et al., 1992; Tse and Hille, 1992), propagating Ca^{2+} waves (Rawlings et al., 1991), and simultaneous behavior of $[Ca^{2+}]_i$ and V (Kukuljian et al., 1992; Li et al., 1995b), and of $[Ca^{2+}]_i$ and $[Ca^{2+}]_{ER}$ (Tse et al., 1994b). These results have enabled us to construct a quantitative model of Ca^{2+} signaling in gonadotrophs to simulate the spatiotemporal behavior of $[Ca^{2+}]_i$, $[Ca^{2+}]_{ER}$, V, and Ca^{2+} fluxes through the ER and plasma membranes, etc.

The experiments and model presented here continue our systematic exploration of Ca^{2+} handling in pituitary gonadotrophs. The model now integrates electrical events at the plasma membrane (millisecond time scale) with IP_3-induced and ER-mediated $[Ca^{2+}]_i$ oscillations (second time scale) to help understand store depletion and refilling (minute time scale). Special efforts have been made at each stage to compare the model with all available experimental observations. For example, the range of free Ca^{2+} concentration in the store has been adjusted to match newly published estimates (Tse et al., 1994b). The quantitative Ca^{2+} fluxes through the plasma membrane, as constrained by whole-cell clamp data (Li et al., 1995b), have provided additional constraints for parameters involved in ER calcium handling (Li et al., 1994).

Our earlier predictions that a single cycle of Ca^{2+} release depletes the ER only fractionally and that many cycles of $[Ca^{2+}]_i$ oscillations are required for significant depletion (Li et al., 1994) have been confirmed by experiments (Tse et al., 1994b; Chatton et al., 1995). On the other hand, how store content is signaled to the plasma membrane to trigger "capacitative" Ca^{2+} entry has not been fully explained in excitable cells that do not express a functional I_{crac}, including gonadotrophs (Kukuljan et al., 1994; McArdle et al., 1996). Results in this paper reveal (Fig. 7), for the first time, a simple mechanism for communication between the ER and the plasma membrane in excitable cells in which $[Ca^{2+}]_i$ itself is the messenger. In this mechanism, net Ca^{2+} flux at the plasma membrane is controlled by the spatiotemporal profile $[Ca^{2+}]_i$, which is determined by the interplay between spontaneous AP spikes and agonist-induced $[Ca^{2+}]_i$ oscillations. During depletion this Ca^{2+} signal increases net Ca^{2+} influx predominantly by reducing the extrusion rate, whereas during refilling it facilitates AP spikes. In contrast to observations in cells that express I_{crac} (Takemura et al., 1989; Zweifach and Lewis, 1993), refilling in gonadotrophs only occurs after the stimulus is withdrawn and when $[Ca^{2+}]_i$ is lower than its unstimulated (basal) level.

The mechanism of Ca^{2+}-controlled Ca^{2+} entry can be understood as follows. In the full-store state (SS-1) $[Ca^{2+}]_i$ is at basal level and the SERCA pump current balances the ER Ca^{2+} leak, while the plasma membrane pump current balances Ca^{2+} entry via voltage-dependent channels. When the ER membrane is made more permeable to Ca^{2+} by increasing $[IP_3]$, the balance at both membranes is broken. Initially ER Ca^{2+} release overwhelms Ca^{2+} uptake and floods the cytosol with Ca^{2+}. The increase in $[Ca^{2+}]_i$ increases Ca^{2+} extrusion via the plasma membrane pumps and hyperpolarizes the plasma membrane by activating $I_{K(Ca)}$, thus reducing voltage-gated Ca^{2+} entry. As store depletion (T-1) proceeds, the amount of ER Ca^{2+} release during each cycle declines, causing a slow decline in average $[Ca^{2+}]_i$, both throughout the cell and at the plasma membrane. The primary effect of this decline is to regulate net plasma membrane exchange by reducing Ca^{2+} extrusion (Fig. 7). When the empty-store state (SS-2) is reached, Ca^{2+} fluxes across each membrane are again in balance and $[Ca^{2+}]_i$ reaches a level near basal (Fig. 3). As compared to SS-1, however, the balance is achieved with IP_3 channels that are more permeable to Ca^{2+} and an ER that has a much lower Ca^{2+} content. When IP_3 is subsequently removed, the

reduction in Ca^{2+} efflux through the ER membrane again breaks the balance. Under these conditions ER Ca^{2+} uptake overwhelms the Ca^{2+} leak, causing a decline in $[Ca^{2+}]_i$ below its basal level (Fig. 3). At the plasma membrane this decline both reduces Ca^{2+} extrusion and depolarizes the plasma membrane by lowering $I_{K(Ca)}$, resulting in an increase in net Ca^{2+} entry and store refilling.

The present study suggests that calcium-controlled calcium entry in gonadotrophs involves two distinct regulatory mechanisms: Ca^{2+}-controlled Ca^{2+} efflux through the plasma membrane (pumps and exhangers) and Ca^{2+}-controlled Ca^{2+} influx through $I_{K(Ca)}$ and voltage-gated Ca^{2+} channels. Experimentally it is possible to dissociate these two mechanisims using voltage clamping, thereby fixing the Ca^{2+} influx rate. In this case, we predict that Ca^{2+}-controlled Ca^{2+} outflow alone regulates store depletion and refilling. Additional studies like those of Tse et al. (1994b) in voltage-clamped gonadotrophs should help shed light on such regulation. In electrically active gonadotrophs, however, Ca^{2+}-controlled Ca^{2+} inflow further reinforces the overall Ca^{2+}-controlled mechanism, by slowing store depletion (during T-1) and accelerating store refilling (T-2).

The model also permits us to simulate the agonist dose response of store depletion (Fig. 4). Agonist dose not only determines the half-depletion time and the extent of store depletion, but also changes the shape of the time course of the individual cycles of ER content during depletion by changing the oscillation frequency. Three features of store depletion are worth noting: 1) At low $[IP_3]$, no detectable Ca^{2+} uptake occurs during the first few $[Ca^{2+}]_i$ spikes immediately after agonist is added. 2) When the depletion is modest and the $[Ca^{2+}]_i$ oscillation frequency is low, $[Ca^{2+}]_{ER}$ drops sharply as $[Ca^{2+}]_i$ peaks, but recovers in two distinct phases: a rapid uptake phase mirroring the $[Ca^{2+}]_i$ downstroke, followed by a slow uptake phase in the interspike interval (as observed by Tse et al., 1994b). 3) When store content is low and the interval between $[Ca^{2+}]_i$ spikes is short, the $[Ca^{2+}]_{ER}$ profile is roughly complementary to the $[Ca^{2+}]_i$ profile (as observed by Chatton et al., 1995; Tanimura and Turner, 1996).

Computations also reveal the essential role of electrical activity in sustaining ER Ca^{2+} excitability (Li et al., 1995b) during prolonged agonist stimulation (Fig. 6). Results here illustrate that AP-driven Ca^{2+} entry is sufficient to compensate for the loss of Ca^{2+} suffered in each massive Ca^{2+} release by the store in low-frequency oscillations (Figs. 4 *A* and 6 *A*). Although the cycling of about 0.11 fmol of Ca^{2+} ions from the ER to the cytosol and to extracellular medium and back to the ER can happen in the absence of other Ca^{2+} stores, these results do not exclude the possibility that a fraction of these Ca^{2+} ions are actually being shuttled from the ER to other compartments and back to the ER. Further improvements in our understanding of the role of mitochondrial Ca^{2+} handling in gonadotrophs and the significance of agonist-induced Ca^{2+} waves should be easy to introduce into future simulations (Jouaville et al., 1995).

In summary, the model not only reproduces the complex dynamic patterns already observed, but also provides estimates for quantities, such as the spatial distribution of $[Ca^{2+}]_i$, that are currently difficult to measure experimentally. Five specific predictions should provide clear experimental tests of the model: 1) the dose dependence of the half-depletion time and the shape of the per-cycle time course of luminal Ca^{2+} during store depletion (Fig. 4 *A*); 2) a substantial decline in $[Ca^{2+}]_i$ below basal level during store refilling (Figs. 3 and 7); 3) large-amplitude $[Ca^{2+}]_i$ oscillations sustained by voltage spiking at low store content (Fig. 6); 4) repetitive pulses of Ca^{2+} release from the ER, although triggered by voltage spikes at the plasma membrane, have maximum amplitude in the interior of the cell (Fig. 6, *A* and *B*); 5) during store refilling AP frequency is markedly increased.

Prediction 5) can be checked with long-term current-clamp measurements. Whereas the decline of $[Ca^{2+}]_i$ after washout of GnRH (prediction 2) may be difficult to measure with fluorescence techniques, indirect measurements using $I_{K(Ca)}$ under voltage-clamp conditions may provide a test (Tse et al., 1994b). The method developed by Tse et al. (1994b) can be used to test 1) under voltage-clamp conditions. To test 1) in the absence of voltage clamp, Ca^{2+} dyes targeted separately to the cytosol and the ER and with distinct wavelengths (Chatton et al., 1995) might be used. Verification of prediction 3) will require long time records and cells with unchanging properties and so may be difficult to achieve. A test of prediction 4), on the other hand, could be made using high-spatial-resolution confocal microscopy (Rawlings et al., 1991) employing either membrane-bound dyes or cytoplasmic Ca^{2+} indicators.

Ca^{2+} mobilization is of primary importance for the secretion of hormones/neurotransmitters in a number of endocrine/neuroendocrine cells, including pituitary gonadotrophs (Stojilković et al., 1990). It is also essential in controlling the synthesis of hormones and the expression of several early- and late-response genes (Stojilković and Catt, 1994). In hippocampal neurons, synaptic activation of the metabotropic glutamate receptor, which triggers intradendritic Ca^{2+} release by producing IP_3 (Jaffe and Brown, 1994), is needed for the induction of long-term potentiation (Katsuki et al., 1992; Bashir et al., 1993). In a modeling study, the induction time course is determined by the store's kinetics of calcium handling (Schiegg et al., 1995). During long-term agonist stimulation, however, the limited reserve of intracellular Ca^{2+} stores could be exhausted in minutes, and that in dendritic spines even more quickly. Thus voltage spiking that promotes Ca^{2+} entry through voltage-gated calcium channels becomes vital for preserving the ER's ability to release Ca^{2+} in large pulse(s) (Stojilković et al., 1992; Jaffe and Brown, 1994). That, in gonadotrophs, Ca^{2+} itself plays the messenger role in reporting the filling state of the ER Ca^{2+} store to the plasma membrane may represent a mechanism that bears more general relevance to other excitable cells.

APPENDIX

Parameter values and functional expressions

The electrical activity of the cell is governed by the voltage equation, $c_m\dot{V} = I_{app} - I_{Ca\text{-}T} - I_{Ca\text{-}L} - I_{K\text{-}DR} - I_{K(Ca)} - I_L$, with the currents defined as $I_{Ca\text{-}T} = g_{Ca\text{-}T}m_T^2h_T\phi_{Ca}(V)$, $I_{Ca\text{-}L} = g_{Ca\text{-}L}m_L^2\phi_{Ca}(V)$, $I_{K\text{-}DR} = g_{K\text{-}DR}n\phi_K(V)$, $I_{K(Ca)} = g_{K(Ca)}C_R^4/(C_R^4 + K_{ca}^4)\phi_K(V)$, and $I_L = g_L(V - V_L)$, where $\phi_X(V) = V[X_i - X_o\exp(-z_XFV/RT)]/[1 - \exp(-z_XFV/RT)]$ is the Goldman-Hodgkin-Katz driving force for the ion X. The gating variables m_T, h_T, m_L, and n are governed by the gating equation $\dot{q} = (q_\infty - q)/\tau_q$, with q representing each of the four gating variables.

The equilibrium gating functions of the plasma membrane ionic channels are $m_{T,\infty} = \Gamma(V_{mt}, V, k_{mt})$, $h_{T,\infty} = \Gamma(V, V_{ht}, k_{ht})$, $m_{L,\infty} = \Gamma(V_{ml}, V, k_{ml})$, $n_\infty = \Gamma(V_{nk}, V, k_{nk})$. The time scales for the corresponding gating variables are (in ms): $\tau_{mt} = 10\tau(V)$, $\tau_{ml} = 30\tau(V)$, $\tau_{ht} = 15$, $\tau_{nk} = 22.5$; with $\tau(V) = 1/(\exp[(V + 60)/22] + 2\exp[-(V + 60)/11])$. Other parameter values are (in mV): $V_{mt} = -30$, $V_{ml} = -12$, $V_{ht} = -50$, $V_{nk} = -5.1$, $k_{mt} = 9$, $k_{ml} = 12$, $k_{ht} = 4$, $k_{nk} = 12.5$, $V_L = -55$; and (in nS/mM): $g_{Ca\text{-}T} = 6.8$, $g_{Ca\text{-}L} = 6.2$, $g_{K\text{-}DR} = 0.1$, $g_{K(Ca)} = 0.01$. Also, $K_{Ca} = 0.6$ μM, $F/(RT) = 0.0375$ mV^{-1}, $c_m = 12.5$ pF, $g_L = 0.008$ nS, $\alpha = 1/(2FA_{cell}) = 4.144$ μM·μm/(s·pA); and (in mM): $\bar{C}_o = 2.5$, $\bar{C}_i = 0.0001$, $\bar{K}_o = 5$, $\bar{K}_i = 140$. These parameter values and functional expressions were obtained from experiments with gonadotrophs, as briefly explained in Materials and Methods. A detailed table containing all of these parameter values together with references specifying their source of origin has previously been published (Li et al., 1995b).

The Ca^{2+} flux densities are defined as $j_{fil} = J_{fil}/(V_{cell}/f_{cyt})$ with $J_{fil} = V_{er,p}C^2/(C^2 + K_{er,p}^2)$; $j_{out} = j_{pm,p} + j_{pm,ex}$ with $j_{pm,p} = \nu_{pm,p}C_R^2/(C_R^2 + K_{pm,p}^2)$ and $j_{pm,ex} = \nu_{pm,ex}C_R^4/(C_R^4 + K_{pm,ex}^4)$, where subscipts pm, p and pm, ex refer to "plasma membrane Ca^{2+} pump" and "plasma membrane Na^+-Ca^{2+} exchanger." $C_R = C(R)$ denotes the $[Ca^{2+}]_i$ at the plasma membrane. $j_{rel} = J_{rel}/(V_{cell}/f_{cyt})$ with $J_{rel} = (P_{leak} + P_{ip3r}O)(C_{er} - C)$. $O = a_\infty b_\infty d_\infty h$, where a_∞ represents the rapid activation of the channel opening by C, b_∞ describes the fast IP_3 activation of the channel, d_∞ determines the channel gating by C_{ER}, and h governs the slow channel inactivation by C. The time evolution of h is described by the gating equation $\dot{h} = (h_\infty - h)/\tau_h$.

The equilibrium gating functions of the IP_3R channels are $a_\infty = \Gamma(\theta_a, C, k_a)$, $b_\infty = \Gamma(\theta_b, IP_3, k_b)$, $d_\infty = 0.2[1 + 4\Gamma(C_{er}, \theta_d, k_4)]$, $h_\infty = \Gamma(C, \theta_h, k_h)$, where

$$\Gamma(x, y, z) = 1/(1 + \exp[(x - y)/z]),$$

$$k_a = \bar{k}_a\left[0.8 + \left(\frac{IP_3}{IP_3 + 0.2}\right)\frac{0.15^2}{0.15^2 + (IP_3 - 0.4)^2}\right] \cdot \left[\frac{60}{60 + C_{er}}\right], \quad k_h = \bar{k}_h\left[0.05 + \frac{IP_3^2}{(IP_3^2 + 1) + 180/C_{er}}\right],$$

$$\text{and } \tau_h = \bar{\tau}_h/(b_\infty d_\infty \cosh[(C - \theta_t)/k_t]).$$

The parameter values are (in μM): $\theta_a = 0.4$, $\theta_b = 0.6$, $\theta_d = 20$, $\theta_h = 0.36$, $\bar{k}_a = 0.14$, $k_b = 0.2$, $k_d = 10$, $\bar{k}_h = 0.46$; and $\bar{\tau}_h = 1.2$ s. Also (in $\mu m^2 \cdot s^{-1}$): $D = 20$, $D_{er} = 5$, $D_0 = 1000$; (in μM) $K_{er,p} = 0.2$, $K_{pm,p} = 0.1$, $K_{pm,ex} = 0.9$; (in μM·μm·s^{-1}) $\nu_{pm,p} = 20$, $\nu_{pm,ex} = 200$; (in pL·s^{-1}) $P_{leak} = 6$, $P_{ip3r} = 750$; and $V_{er,p} = 750$ μM·pL·s^{-1}. As explained briefly in Materials and Methods, these parameter values and functional expressions are partly based on experiments in other cell types (see Li et al., 1994, for detail) but are constrained through coupling with the more accurate plasma membrane model, to systematically reproduce the whole spectrum of dynamic dose responses.

The cytosolic volume is approximated by the whole cell volume, $V_{cell} = 4.2$ pl, whereas the ER volume is assumed to be 15% of V_{cell} (see Alberts et al., 1989), i.e. $V_{er} = 0.63$ pl. $\sigma = (V_{er}/f_{er})/(V_{cell}/f_{cyt}) = 0.6$, where $f_{er} = 0.0025$ and $f_{cyt} = 0.01$ (Tse et al., 1994a).

This work was partially supported by funds from NSF grants BIR 9234381 and BIR 9300799 and PHS grant R01 RR1081-01A1 (to JK) and the Agricultural Experiment Station at UC Davis.

REFERENCES

Alberts, B., D. Bray, J. Lewis, M. Raff, K. Roberts, and J. D. Watson. 1989. Molecular Biology of the Cell, 2nd Ed. Garland, New York. 406–407.

Allbritton, N., T. Meyer, and L. Stryer. 1992. Range of messenger action of calcium ion and inositol 1,4,5-trisphosphate. *Science.* 258: 1812–1815.

Bashir, Z. I., Z. A. Bortolotto, C. H. Davies, N. Berretta, A. J. Irving, A. J. Seal, J. M. Henley, D. E. Jane, J. C. Watkins, and G. L. Collingdrige. 1993. Induction of LTP in the hippocampus needs synaptic activation of glutamate metabotropic receptors. *Nature.* 363:347–350.

Berridge, M. J. 1993. Inositol trisphosphate and calcium signalling. *Nature.* 361:315–325.

Berridge, M. J. 1995. Capacitative calcium entry. *Biochem. J.* 312:1–11.

Bezprozvanny, I., J. Watras, and B. E. Ehrlich. 1991. Bell-shaped calcium response curves of Ins(1,4,5)P_3- and calcium-gated channels from endoplasmic reticulum of cerebellum. *Nature.* 351:751–754.

Bootman, M. D. 1994. Quantal Ca^{2+} release from $InsP_3$-sensitive intracellular Ca^{2+} stores. *Mol. Cell. Endocrinol.* 98:157–166.

Casteels, R., and G. Droogmans. 1981. Exchange characteristics of the noradrenaline-sensitive calcium store in vascular smooth muscle cells of rabbit ear artery. *J. Physiol. (Lond.).* 317:263–279.

Chatton, J. Y., H. Liu, and J. W. Stucki. 1995. Simultaneous measurements of Ca^{2+} in the intracellular stores and the cytosol of hepatocytes during hormone-induced Ca^{2+} oscillations. *FEBS Lett.* 368:165–168.

De Young, G., and J. Keizer. 1992. A single-pool inositol 1,4,5-trisphosphate-recepter-based model for agonist-stimulated oscillations in Ca^{2+} concentration. *Proc. Natl. Acad. Sci. USA.* 89:9895–9899.

Hoth, M., and R. Penner. 1992. Depletion of intracellular calcium stores activates a calcium current in mast cells. *Nature.* 355:353–356.

Iida, T., S. S. Stojilković, S. Izumi, and K. J. Catt. 1991. Spontaneous and agonist-induced calcium oscillations in pituitary gonadotrophs. *Mol. Endocrinol.* 5:949–958.

Iino, M. 1990. Biphasic Ca^{2+}-dependence of inositol 1,4,5-trisphosphate-induced Ca^{2+} release in smooth muscle cells of the guinea pig *Taenia caeci. J. Gen. Physiol.* 95:1103–1122.

Jaffe, D. B., and T. H. Brown. 1994. Metabotropic glutamate receptor activiation induces calcium waves within hippocampal dendrites. *J. Neurophysiol.* 72:471–474.

Jouaville, L. S., F. Ichas, E. L. Holmuhamedov, P. Camacho, and J. D. Lechleiter. 1995. Synchronization of calcium waves by mitochondrial substrates in *Xenopus laevis* oocytes. *Nature.* 377:438–441.

Katsuki, H., H. Saito, and M. Satoh. 1992. The involvement of muscarinic, beta-adrenergic and metabotropic glutamate receptors in long-term potentiation in the fimbria-CA pathway of the hippocampus. *Neurosci. Lett.* 142:249–252.

Kukuljan, M., E. Rojas, K. J. Catt, and S. S. Stojilković. 1994. Membrane potential regulates inositol 1,4,5-trisphosphate-controlled cytoplasmic Ca^{2+} oscillations in pituitary gonadotrophs. *J. Biol. Chem.* 269: 4860–4865.

Kukuljan, M., S. S. Stojilković, E. Rojas, and K. J. Catt. 1992. Apamin-sensitive potassium channels mediate agonist-induced oscillations of membrane potential in pituitary gonadotrophs. *FEBS Lett.* 301:19–22.

Leong, D., and M. D. Thorner. 1991. A potential code of LHRH-induced calcium ion responses in the regulation of luteinizing hormone secretion among individual gonadotrophs. *J. Biol. Chem.* 266:9016–9022.

Li, Y.-X., J. Keizer, S. S. Stojilković, and J. Rinzel. 1995a. Ca^{2+} excitability of the ER membrane: an explanation for IP_3-induced Ca^{2+} oscillations. *Am. J. Physiol.* 269:C1079–C1092.

Li, Y.-X., J. Rinzel, J. Keizer, and S. S. Stojilković. 1994. Calcium oscillations in pituitary gonadotrophs: comparison of experiment and theory. *Proc. Natl. Acad. Sci. USA.* 91:58–62.

Li, Y.-X., J. Rinzel, L. Vergara, and S. S. Stojilković. 1995b. Spontaneous electrical and calcium oscillations in unstimulated pituitary gonadotrophs. *Biophys. J.* 69:785–795.

Lin, C., G. Hajnóczy, and A. P. Thomas. 1994. Propogation of cytosolic calcium waves into the nuclei of hepatocytes. *Cell Calcium.* 16:247–256.

McArdle, C. A., W. Forrest-Owen, J. S. Davidson, R. Fowkes, R. Bunting, W. T. Mason, A. Poch, and M. Kratzmeier. 1996. Ca^{2+} entry in gonadotrophs and αT3–1 cells: does store-dependent Ca^{2+} influx mediate gonadotrophin-releasing hormone action? *J. Endocrinol.* 149:155–169.

Morgan, R. O., J. P. Chang, and K. J. Catt. 1987. Novel aspects of gonadotropin-releasing hormone action on inositol polyphosphate metabolism in cultured pituitary gonadotrophs. *J. Biol. Chem.* 262: 1166–1171.

Putney, J. W., Jr. 1986. A model for receptor-regulated calcium entry. *Cell Calcium.* 7:1–12.

Rawlings, S. R., D. J. Berry, and D. A. Leong. 1991. Evidence for localized calcium mobilization and influx in single rat gonadotropes. *J. Biol. Chem.* 266:22755–22760.

Schiegg, A., W. Gerstner, R. Ritz, and J. L. van Hemmen. 1995. Intracellular Ca^{2+} stores can account for the time course of LTP induction: a model of Ca^{2+} dynamics in dendritic spines. *J. Neurophysiol.* 74: 1046–1055.

Shangold, G. A., S. N. Murphy, and R. J. Miller. 1988. Gonadotropin-releasing hormone-induced Ca^{2+} transients in single identified gonadotropes require both intracellular Ca^{2+} mobilization and Ca^{2+} influx. *Proc. Natl. Acad. Sci. USA.* 85:6566–6570.

Stojilković, S. S., and K. J. Catt. 1994. Gonadotropin-releasing hormone receptors: structure and signal transduction pathways. *Endocr. Rev.* 15:462–499.

Stojilković, S. S., M. Kukuljan, T. Iida, E. Rojas, and K. J. Catt. 1992. Integration of cytoplasmic calcium and membrane potential oscillations maintains calcium signaling in pituitary gonadotrophs. *Proc. Natl. Acad. Sci. USA.* 89:4081–4085.

Stojilković, S. S., M. Kukuljan, M. Tomic, E. Rojas, and K. J. Catt. 1993. Mechanism of agonist-induced $[Ca^{2+}]_i$ oscillations in pituitary gonadotrophs. *J. Biol. Chem.* 268:7713–7720.

Stojilković, S. S., A. Stutzin, S. Izumi, S. Dufour, A. Torsello, M. A. Virmani, E. Rojas, and K. J. Catt. 1990. Generation and amplification of the cytosolic calcium signal during secretory responses to gonadotropin-releasing hormone. *New Biologist.* 2:272–283.

Stojilković, S. S., M. Tomic, M. Kukuljan, and K. J. Catt. 1994. Control of calcium spiking frequency in pituitary gonadotrophs by a single-pool cytoplasmic oscillator. *Mol. Pharmacol.* 45:1013–1021.

Stutzin, A., S. S. Stojilković, K. J. Catt, and E. Rojas. 1989. Characteristics of two calcium channels in rat pituitary gonadotrophs. *Cell Physiol.* 26:C865–C874.

Takemura, H., A. R. Hughes, O. Thastrup, and J. W. Putney, Jr. 1989. Activation of calcium entry by the tumor promoter thapsigargin in parotid acinar cells. *J. Biol. Chem.* 264:12266–12271.

Tanimura, A., and R. J. Turner. 1996. IP_3-dependent oscillations of luminal $[Ca^{2+}]$ in permeablized HSY cells. *J. Biol. Chem.* 271:30904–30908.

Tse, A., and B. Hille. 1992. GnRH-induced Ca^{2+} oscillations and rhythmic hyperpolarizations of pituitary gonadotropes. *Science.* 255:462–464.

Tse, A., and B. Hille. 1993. Role of voltage-gated Na^+ and Ca^{2+} channels in gonadotropin-releasing hormone-induced membrane potential changes in identified rat gonadotrophs. *Endocrinology.* 132:1472–1481.

Tse, A., F. W. Tse, and B. Hille. 1994a. Calcium homoestasis in identified rat gonadotropes. *J. Physiol. (Lond.).* 477:511–525.

Tse, F. W., A. Tse, and B. Hille. 1994b. Cyclic Ca^{2+} changes in intracellular stores of gonadotropes during gonadotropin-releasing hormone-stimulated Ca^{2+} oscillations. *Proc. Natl. Acad. Sci. USA.* 91: 9750–9754.

Zweifach, A., and R. S. Lewis. 1993. Mitogen-regulated Ca^{2+} current of T lymphocytes is activated by depletion of intracellular Ca^{2+} stores. *Proc. Natl. Acad. Sci. USA.* 90:6295–6299.